(e,$2e$) study on distorted-wave and relativistic effects in the inner-shell ionization processes of xenon $4d_{5/2}$ and $4d_{3/2}$

X. G. Ren, C. G. Ning, J. K. Deng,* G. L. Su, S. F. Zhang, and Y. R. Huang

Department of Physics and Key Laboratory of Atomic and Molecular NanoSciences of MOE, Tsinghua University, Beijing 100084, People's Republic of China

(Received 21 December 2005; published 21 April 2006)

Inner-shell ionization of xenon $4d$ electrons have been studied by the binary (e,$2e$) spectroscopy at the impact energies of 1200, 1600, and 2400 eV. Experimental energy-momentum densities and the impact-energy dependence of momentum distributions of $4d_{5/2}$ and $4d_{3/2}$ are reported, the results are compared with the distorted-wave impulse approximation and the distorted-wave Born approximation. Moreover, the cross-section ratios of $4d_{5/2}$ to $4d_{3/2}$ are further provided at these different impact energies, which clearly manifest the relativistic effects. Some similarities and dissimilarities are observed on the impact-energy dependence of momentum distributions of $4d_{5/2}$ and $4d_{3/2}$ states and their cross-section ratios.

I. INTRODUCTION

Electron impact ionization (e,$2e$) experiments have been successfully used in the last 30 years to obtain fundamental information on the dynamics of the ionization process [1], and as a direct measurement of the target initial state one-electron wave function in momentum space, $|\psi(p)|^2$, via the so-called electron momentum spectroscopy (EMS) or the binary (e,$2e$) spectroscopy [2]. It is now a well-established technique to investigate the atomic and molecular electronic structures and electron correlations [2–6]. Within the kinematically complete ionization process, the ion recoil momentum q and the electron binding energy can be determined by the coincident detections of the two outgoing electrons with the aid of the momentum and energy conservation laws. Under the assumption of binary encounter, Born-Oppenheimer approximation and the further plane-wave impulse approximation (PWIA), the EMS cross section at high energy and high momentum transfer is given by the overlap of the initial neutral (N electron) wave function of $|\Psi_i^N\rangle$ and the final ion ($N-1$ electron) wave function of $|\Psi_f^{N-1}\rangle$ [2,7],

$$\sigma_{EMS} \propto \int |\langle p\Psi_f^{N-1}|\Psi_i^N\rangle|^2 d\Omega, \qquad (1)$$

where p is the momentum of the target electron prior to electron ejection. The $\int d\Omega$ represents the spherical average due to the randomly oriented gas phase target in the collision region. The versatile information for the detailed studies of electronic structure, such as symmetries, binding energy, pole strengths, and electron momentum distributions of the states involved are given by the EMS cross-section measurements.

Most of previous experiments were limited to the studies of valence shell of low- and medium-Z atoms and molecules due to the lower sensitivity and resolutions of instruments.

The scarcity of studies for inner-shell or core states [2,8,9] could be accounted for by the experimental difficulties, which include the extremely small cross sections and the limited sensitivity of the spectrometers, and some complexities in theoretical calculations. Recently, a new type of energy- and momentum-dispersive EMS spectrometer has been developed [10], which features high sensitivity and high resolutions. With double toroidal analyzer and two dimensions position sensitive detectors, the instruments sensitivity or count rate is about two orders of magnitude higher than our previous energy-dispersive spectrometer [11]. The typical energy resolution of 1.2 eV, and the θ and ϕ angle resolutions of $\pm 0.7°$ and $\pm 1.9°$ are achieved with the measurements of argon and helium. Besides the simultaneously obtained high sensitivity and high resolutions performances, another advantage of this spectrometer is its ability to measure the (e,$2e$) cross sections over a wide range of experimental impact energies, which is especially important for systematically investigating some dynamics processes which are energy dependent [12,13]. Using this spectrometer, some new and extended studies have been reported, which include the studies of distorted-wave effects and the validities of theoretical approximations [12,14–16], a new method to determine pole strengths and orbital ordering [17], and electron correlation effects study on helium [18].

In this work, we study the (e,$2e$) cross sections for xenon inner-shell $4d_{5/2}$ and $4d_{3/2}$ states at the impact energies of 1200, 1600, and 2400 eV, and give the remarkable distorted-wave effects in the ionization process and the relativistic effects. Distorted-wave effects in the inner-shell ionization are clearly observed with the impact-energy dependence of momentum distributions of $4d_{5/2}$ and $4d_{3/2}$ states. Moreover, the cross-section ratios of $4d_{5/2}$ to $4d_{3/2}$ provide the detailed information of the relativistic effects on xenon. This paper investigates the inner-shell ionization at a wide range of impact energies using the binary (e,$2e$) method.

II. EXPERIMENT AND REACTION THEORY

EMS is a high-energy electron impact ionization experiment in which the kinematics of all the electrons are fully

*Corresponding author. Electronic mail: djk-dmp@mail.tsinghua.edu.cn

determined. Measuring the energies and momenta of the incident (E_0, p_0) and two outgoing electrons $(E_1, p_1$ and $E_2, p_2)$ can determine the measurements of the target electron binding energy and recoil momentum. One of the mostly used kinematic geometries for EMS is non-coplanar symmetric geometry. In this kinematics, two outgoing electrons have equal scattering polar angles $(\theta_1 = \theta_2 = 45°)$ and energies $(E_1 \approx E_2)$. The magnitude of the recoil ion momentum q can be determined by the measurement of the out-of-plane azimuthal angle difference between the two outgoing electrons [2,10]. In PWIA, the momentum p of the ejected electron prior to knockout is equal in magnitude but opposite in sign to the momentum of the recoiling ion. The magnitude of the momentum p is related to the azimuthal angle difference of ϕ,

$$ p = \left\{ (2p_1 \cos\theta - p_0)^2 + \left[2p_1 \sin\theta \sin\left(\frac{\phi}{2}\right) \right]^2 \right\}^{1/2}, \quad (2) $$

where p_1 and p_0 are the momenta of the outgoing and incident electrons, respectively. Within the PWIA, the EMS cross section is given by the overlap of the ion and neutral wave functions as shown in Eq. (1). The momentum space target-ion overlap can be evaluated by using configuration-interaction (CI) descriptions of the many-body wave functions or Green's function (GF) methods [19].

A detailed description of the spectrometer used in the present work has been given before [10], thus only a brief introduction is provided. In our $(e, 2e)$ experiment, an incident electron beam is produced by an electron gun equipped with a tungsten filament. After the incident electron beam collides with targets, the outgoing scattered and ejected electrons are decelerated by the cone lenses before entering the double toroidal analyzer (DTA) in order to achieve higher energy resolution. Then the two outgoing electrons are energy analyzed and dispersed by the DTA, and detected by a pair of two-dimensional position sensitive detectors. Since the DTA can well maintain the azimuthal angles of the passing electrons, both energies and angles can be simultaneously determined by their arrival positions at the detectors. The experiments are carried out at the impact energies of 1200, 1600, and 2400 eV with 100 eV passing energy in the analyzer.

III. RESULTS AND DISCUSSIONS

A. Energy-momentum density

One typical experimental result of the electron density map for xenon inner-shell $4d$ states is obtained and shown in Fig. 1 as a function of binding energy and azimuthal angle difference of ϕ (also electron momentum p), which is measured at the impact energy of 1600 eV. This contour image represents energy-momentum density of inner-shell electrons and contains a wealth of information on relative intensities, momentum distribution, and symmetries of the states involved. It can be seen that the $4d_{5/2}$ and $4d_{3/2}$ states are well resolved in the energy-momentum density map. The individual momentum distributions of $4d_{5/2}$ and $4d_{3/2}$ states can be obtained by summing up the intensities along the ϕ angle
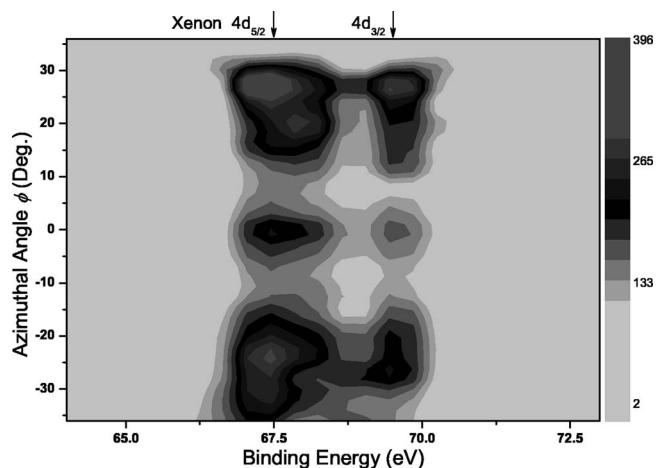

FIG. 1. Experimental energy and angle ϕ (also electron momentum p) density of xenon inner-shell $4d$ states, obtained at the impact energy of 1600 eV.

or momentum p direction at the corresponding binding-energy range in the map.

Furthermore, significant turn up effects at the low momentum (small ϕ angle) region of $4d_{5/2}$ and $4d_{3/2}$ states are clear observed from the experimental energy-momentum density map, which is due to the continuum waves associated with the ionization of $4d$ electrons are distorted from plane waves, also called the distorted-wave effects [2,8,9]. Since the distorted-wave effects largely depend on the impact energy [13], the experiments were performed at a wide range of impact energies to systematically study the distortion effects in the ionization process of xenon inner-shell $4d$ electrons.

B. Momentum distributions

Experimental momentum distributions for low- and medium-Z atoms and molecules are found to be in good agreement with those theoretical descriptions by the nonrelativistic calculations [2,3]. In the case of xenon, the relativistic effects will manifest more remarkably. The EMS studies on the xenon valence shell $5p$, $5s$ and satellites states have been carried out before [20–23]. In the case of inner-shell $4d_{5/2}$ and $4d_{3/2}$ states, the distorted-wave effects also become significant at the low momentum region [8,9]. The measurements of xenon $4d$ momentum distribution have been previously made by Brunger *et al.* [9] and Brion *et al.* [8] at the impact energies of 1000 and 1200 eV, respectively. Since the limitation of instruments sensitivity, only the total $4d$ cross-section profiles were obtained for improving the statistical quality of the derived momentum distributions.

With our new EMS spectrometer, the experimental momentum distributions on the individual $4d_{5/2}$ and $4d_{3/2}$ states were measured at the impact energies of 1200, 1600, and 2400 eV as shown in Figs. 2 and 3, respectively. Also included in the figures are the distorted-wave impulse approximation (DWIA) [8] and distorted-wave Born approximation (DWBA) [9] calculations under the nonrelativistic theory, which were digitized from the literatures and normalized to the experimental data. As shown in Figs. 2 and 3, the DWBA
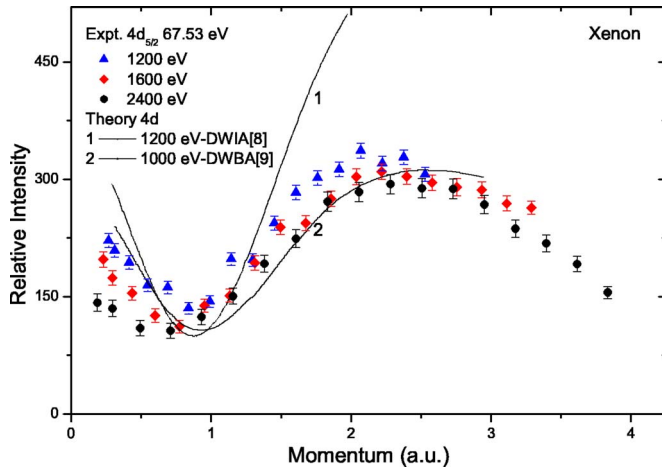
FIG. 2. (Color online) Experimental momentum distributions of xenon inner-shell $4d_{5/2}$ state measured at the impact energies of 1200, 1600, and 2400 eV. The solid lines are the distorted-wave nonrelativistic calculations of DWIA and DWBA.

and DWIA methods can provide somewhat good descriptions of the turn up effects at the low momentum region, which become smaller at the higher impact energies. Such phenomenon is consistent with the distorted-wave predictions at the low momentum region of atomic Cr $3d$, Zn $3d$, Mo $4d$, and Cd $4d$ momentum distributions [8]. With the impact-energy dependence of momentum distributions of $4d_{5/2}$ and $4d_{3/2}$ states, the distorted-wave explanation for the cross-section turn up effects become more convincing for the atomic nd electrons ionized.

It also should be noted that DWBA method reproduces the $4d_{5/2}$ and $4d_{3/2}$ momentum distributions better than DWIA does. Nevertheless, there are some differences between the DWBA calculation and the experimental data. Experimental momentum distributions indicates that the DWBA calculation underestimate the momentum distribution intensity at the region of 1.0 a.u. $< p <$ 1.6 a.u., and the
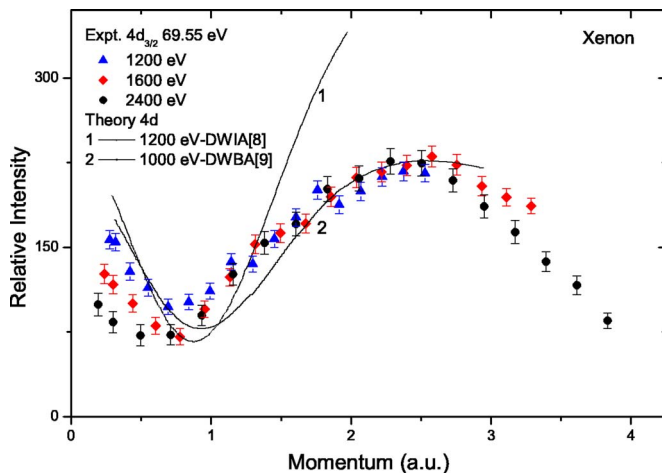

FIG. 3. (Color online) Experimental momentum distributions of xenon inner-shell $4d_{3/2}$ state measured at the impact energies of 1200, 1600, and 2400 eV. The solid lines are the distorted-wave nonrelativistic calculations of DWIA and DWBA.
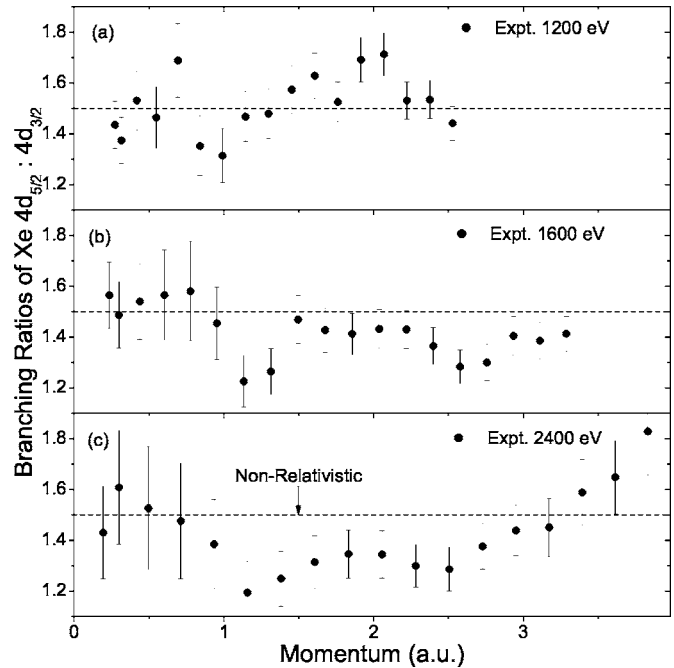

FIG. 4. Cross-section ratios of xenon $4d_{5/2}$ to $4d_{3/2}$ measured at different impact energies of (a) 1200 eV, (b) 1600 eV, and (c) 2400 eV.

first minimum in the cross section is at a smaller value of momentum than the DWBA indicates [9]. At the higher than 2.5 a.u. momentum region some discrepancies are also remarkable. These discrepancies indicate that the DWBA and DWIA calculations need to be improved and the relativistic effects also should be included in the calculations of xenon $4d_{5/2}$ and $4d_{3/2}$ states. Furthermore, comparisons between $4d_{5/2}$ and $4d_{3/2}$ states show somewhat discrepancies in the shape of the experimental momentum distributions, which could be due to the influence of relativistic effects in the inner-shell of xenon [24].

C. Cross-sections ratios

The relativistic effects in the xenon $4d$ states can be sensitively observed by plotting the $(e,2e)$ cross-section ratios of $4d_{5/2}$ to $4d_{3/2}$ versus the momentum p. Since the nonrelativistic structure theories predict that the cross-section ratio of $4d_{5/2}$ to $4d_{3/2}$ should be independent to the momentum p, while the ratio should be given simply by the relative statistical weights of $(2j+1)$, namely 3:2. Figure 4 shows the experimental ratios of $4d_{5/2}$ to $4d_{3/2}$ obtained at the impact energies of 1200, 1600, and 2400 eV, in which the cross sections of $4d_{5/2}$ and $4d_{3/2}$ states were measured at the same azimuthal angle difference of ϕ, and not at the same values of p, since the different binding energies give slightly different values of p with the same values of ϕ as described by Eq. (2). Therefore interpolated cross sections of $4d_{5/2}$ were used in driving the $4d_{5/2}$ to $4d_{3/2}$ ratios. As the dashed line showed in Fig. 4, the nonrelativistic theory predicted a constant ratio of 1.5, which totally failed to reproduce the variation of the experimental ratios. This indicates the significant influence of relativistic effects in xenon inner-shell $4d$ states.

It can be seen from Fig. 4 that the shape of branching ratios of $4d_{5/2}$ to $4d_{3/2}$ are quite similar with the variations of impact energies. However, the relative intensities of the cross-section ratios largely depend on the impact energy, especially at the momentum range of 1.2 a.u.$< p <$2.6 a.u. the ratio intensities become smaller with the increase of the impact energies.

IV. SUMMARY

This study reported the binary $(e, 2e)$ measurements on the inner-shell of xenon $4d$ electrons at the impact energies of 1200, 1600, and 2400 eV. The experimental momentum distributions of $4d_{5/2}$ and $4d_{3/2}$ states clearly show significant variations in the low momentum region with increasing impact energy. The distorted-wave calculations give appropriate description of the cross-section turn up at the low momentum region. Further comparisons between experimental results and distorted-wave calculations indicate that the DWBA method reproduces well the momentum distributions of the $4d$ electrons. Moreover, the cross-section ratios of $4d_{5/2}$ to $4d_{3/2}$ clearly manifest the remarkable influences of relativistic effects in the xenon. The fact that the ratios are so dependent on impact energy shows that distortion effects are quite important in the relative cross sections of $(e, 2e)$ reaction on xenon $4d$ states.

[1] A. Lahmam-Bennani, J. Phys. B **24**, 2401 (1991).

[2] I. E. McCarthy and E. Weigold, Rep. Prog. Phys. **54**, 789 (1991).

[3] C. E. Brion, Int. J. Quantum Chem. **29**, 1397 (1986).

[4] M. A. Coplan, J. H. Moore, and J. P. Doering, Rev. Mod. Phys. **66**, 985 (1994).

[5] V. G. Neudatchin, Yu. V. Popov, and Yu. V. Smirnov, Phys. Usp. **42**, 1017 (1999).

[6] A. Lahmam-Bennani, J. Electron Spectrosc. Relat. Phenom. **123**, 365 (2002).

[7] M. J. Brunger and W. Adcock, J. Chem. Soc., Perkin Trans. 2 **2002**, 1 (2002).

[8] C. E. Brion, Y. Zheng, J. Rolke, J. J. Neville, I. E. McCarthy, and J. Wang, J. Phys. B **31**, L223 (1998).

[9] M. J. Brunger, S. W. Braidwood, I. E. McCarthy, and E. Weigold, J. Phys. B **27**, L597 (1994).

[10] X. G. Ren, C. G. Ning, J. K. Deng, S. F. Zhang, G. L. Su, F. Huang, and G. Q. Li, Rev. Sci. Instrum. **76**, 063103 (2005).

[11] J. K. Deng, G. Q. Li, Y. He, J. D. Huang, H. Deng, X. D. Wang, F. Wang, Y. A. Zhang, C. G. Ning, N. F. Gao, Y. Wang, X. J. Chen, and Y. Zheng, J. Chem. Phys. **114**, 882 (2001).

[12] X. G. Ren, C. G. Ning, J. K. Deng, S. F. Zhang, G. L. Su, F. Huang, and G. Q. Li, Phys. Rev. Lett. **94**, 163201 (2005).

[13] C. E. Brion, G. Cooper, R. Feng, S. Tixier, Y. Zheng, I. E. McCarthy, Z. Shi, and S. Wolfe, in *Correlations, Polarization,*

and Ionization in Atomic Systems, edited by D. Madison and M. Schulz, AIP Conf. Proc. 604 (AIP, New York, 2002), p. 38.

[14] X. G. Ren, C. G. Ning, J. K. Deng, S. F. Zhang, G. L. Su, F. Huang, and G. Q. Li, Chem. Phys. Lett. **404**, 279 (2005).

[15] X. G. Ren, C. G. Ning, J. K. Deng, S. F. Zhang, G. L. Su, Y. R. Huang, and G. Q. Li, J. Electron Spectrosc. Relat. Phenom. **151**, 92 (2006).

[16] C. G. Ning, X. G. Ren, J. K. Deng, S. F. Zhang, G. L. Su, F. Huang, and G. Q. Li, Chem. Phys. Lett. **407**, 423 (2005).

[17] C. G. Ning, X. G. Ren, J. K. Deng, S. F. Zhang, G. L. Su, F. Huang, and G. Q. Li, J. Chem. Phys. **122**, 224302 (2005).

[18] X. G. Ren, C. G. Ning, J. K. Deng, G. L. Su, S. F. Zhang, Y. R. Huang, and G. Q. Li, Phys. Rev. A **72**, 042718 (2005).

[19] C. G. Ning, X. G. Ren, J. K. Deng, G. L. Su, S. F. Zhang, S. Knippenberg, and M. S. Deleuze, Chem. Phys. Lett. **421**, 52 (2006).

[20] A. J. Dixon, I. E. McCarthy, C. J. Noble, and E. Weigold, Phys. Rev. A **17**, 597 (1978).

[21] J. P. D. Cook, I. E. McCarthy, J. Mitroy, and E. Weigold, Phys. Rev. A **33**, 211 (1986).

[22] S. Braidwood, M. Brunger, and E. Weigold, Phys. Rev. A **47**, 2927 (1993).

[23] J. P. D. Cook, J. Mitroy, and E. Weigold, Phys. Rev. Lett. **52**, 1116 (1984).

[24] W. Nakel and C. T. Whelan, Phys. Rep. **315**, 409 (1999).